44th AIAA Plasmadynamics and Lasers Conference
24-27 June 2013, San Diego, CA
AIAA-2013-3137

The Comparison of Unsteady Pressure Field over Flat- and Conformal-Window Turrets using Pressure Sensitive Paint

Stanislav Gordeyev[1], Nicholas De Lucca[2], Eric Jumper[3]
University of Notre Dame, Notre Dame, Indiana 46545, USA

Kyle Hird[4], Thomas J. Juliano[5], James W. Gregory[6]
The Ohio State University, Columbus, Ohio 43235, USA

James Thordahl[7] and Donald J. Wittich[8]
Air Force Research Laboratory, Directed Energy Directorate, Kirtland AFB, NM 87117

Spatially-temporally-resolved unsteady pressure fields on a surface of a hemisphere-on-cylinder turret with either a flat- or a conformal-window were characterized using fast-response pressure sensitive paint at M = 0.33 for several window viewing angles. Various statistical properties of pressure fields were computed and geometry effects on unsteady pressure, including an effect of either flat- or conformal-window, were analyzed and discussed. Proper orthogonal decomposition were also used to extract dominant pressure modes and corresponding temporal coefficients and to analyze and compare instantaneous pressure structures for different turret geometries and viewing angles. In addition, the effects of gaps and 'smile' cut-outs present on the turret were investigated.

Introduction

The hemisphere-on-cylinder turret is a common geometry for either directed energy or free-space communication systems to maximize the potential field-of-regard. The turret geometry has been previously shown to feature a highly three-dimensional turbulent flow field [1], shown schematically in Figure 1. This three-dimensional turbulent flow field has the effect of limiting the effective field-of-regard of the turret, as turbulent regions of compressible flow introduce aberrations in the incident laser beam [1]. The hemisphere-on-cylinder turret has been studied extensively in recent years. There has been a large parametric study of the aero-optical properties of this geometry in flight using the Airborne Aero-Optics Laboratory, AAOL [2,3]. Additionally a variety of CFD studies have been performed on the turret geometry [4-7]. Finally, various flow control mechanisms have been studied on this geometry [7,8,9]. There has also been substantial research into the difference in aero-optical performance between flat and conformal windows on turrets [1,2].

As the turret is not a rigid body, its motion can introduce a jitter into a laser projected from it. From a practical perspective, a jitter of only a few microradians can force a beam to miss a distant target. One source of turret vibrations arises from pressure fluctuations that are due to the turbulent flow features around the turret. The beam jitter related to these flow-induced vibrations is termed the aero-mechanical jitter of the turret. While the turret vibrational response depends on an internal structure, an unsteady pressure field depends only on the turret geometry

[1] Research Associate Professor, Department of Aerospace and Mechanical Engineering, Hessert Laboratory for Aerospace Research, AIAA Associate Fellow.
[2] Graduate Student, Department of Aerospace and Mechanical Engineering, Hessert Laboratory for Aerospace Research, AIAA Student Member.
[3] Professor, Department of Mechanical and Aerospace Engineering, Hessert Laboratory for Aerospace Research, Notre Dame, IN 46556, AIAA Fellow.
[4] Undergraduate Research Assistant, Department of Mechanical and Aerospace Engineering, 2300 West Case Rd.
[5] Postdoctoral Research Associate, Department of Mechanical and Aerospace Engineering, 2300 West Case Rd., AIAA Member. Currently NRC Postdoctoral Research Fellow at Air Force Research Laboratory, Wright-Patterson AFB, OH.
[6] Assistant Professor, Department of Mechanical and Aerospace Engineering, 2300 West Case Rd., AIAA Senior Member.
[7] Sr. Project Engineer, The Aerospace Corporation, 2155 Louisiana Blvd, Suite 5000, Albuquerque, NM 87110
[8] Aerospace Engineer, Laser Division, 3550 Aberdeen Ave SE

and the incoming Mach number. In addition, unsteady pressure fluctuations on the surface of the turret are directly related to the turbulent structures, causing aero-optical global jitter and higher-order aberrations [10].

One way to investigate time-changing pressure field on the surface of the turret is to use an array of unsteady pressure sensors, although in practice it usually it gives a fairly coarse spatial resolution. Another alternative is to use a pressure-sensitive paint, PSP [11], where, by nature of the technique, a very detailed spatial resolution can be achieved. While PSP technique was been known since 1980s, its temporal response was very low, so results were limited to mostly steady-state pressure distributions. Recent advances in development of fast-response porous PSP coatings [12] allowed one to increase PSP frequency response up to several kilohertz [13,14]. Using fast-response PSP, unsteady pressure field around a hemispherical turret at transonic speeds, including dynamics of the unsteady shock on top of the turret, was investigated in [14,15].

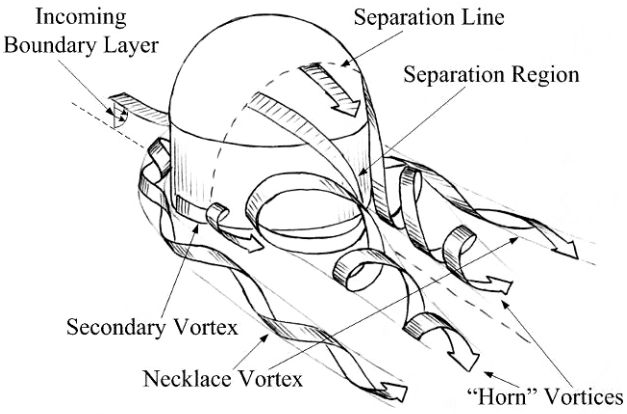

Figure 1. Schematic of the flow around the hemisphere-on-cylinder turret. From [1].

This paper presents and analyzes experimental results obtained using fast-response PSP to study the unsteady pressure fields for different turret geometries at subsonic speeds. Extensive experimental database was analyzed by applying a Proper Orthogonal Decomposition (POD) and dominant pressure modes and their temporal coefficients were extracted and discussed for different turret geometries and window viewing angles. A joint POD technique was also introduced and illustrated to provide a rigorous framework of comparing unsteady pressure fields for different geometries.

Experimental Setup

The tested hemisphere-on-cylinder turret model, with a diameter, D, of 30.5 cm and a cylindrical base height of H = 11.1 cm, was an exact replica of AAOL turret shell, shown in Figure 2 used for aero-optical flight tests [16]. The turret has a rotating portion, or a "donut", allowing to continuously change the elevation angle of the window and the whole turret assemble can be rotated to any azimuthal angle. The turret has several realistic features, like 1-mm gaps between the rotating portion of the turret and trunnions, as well as cut-outs, or "smiles", on both sides of the stationary portion of the turret, typically used to increase filed-of-regard at low elevation angles.

A complete description of the PSP tests is presented in [17], so only essential details will be provided in this paper. The polymer-ceramic/PtTFPP paint with a frequency response up to at least 6 kHz was used [12]. The pressure sensitive paint measurements were acquired in the White Field wind tunnel at the University of Notre Dame, see Figure 3. The wind tunnel is a closed-return tunnel with a 0.9m x 0.9m test section and capable of test section speeds to up Mach number of 0.6. In this test, data were acquired at M = 0.33. The turret assembly allowed a continuous variation in both azimuthal and elevation angles. Additionally, the window could be switched between a flat window and a conformal one; the diameter of the flat portion of the window was 10 cm or D/3. Figure 4 presents a picture and a schematic of the layout of the experimental hardware. Three cameras, one on each side of the test section and one on the top, were used to capture the entire turret surface, allowing resolving the unsteady pressure field on the turret. The three cameras acquired frames at 2000 Hz for 2.75 seconds. Relevant details about each camera are given in Table 1. The turret was imaged twice using the high-speed cameras for wind-off and wind-on conditions, which is a characteristic procedure for PSP measurements. 5750 frames were taken with the eight UV LED arrays, four LEDs on both sides of the test section, illuminating the entire surface of the model.

Additionally, as shown in Figure 2, bottom plots, eight unsteady pressure Kulite sensors were used to verify the time-variation of the PSP data and to provide a reference pressure for post-process analysis. The pressure sensors were referenced to the interior pressure of the turret, which was measured with an external system. To complement the pressure sensors, five thermocouples were placed on the surface of the turret, see Figure 2, bottom plots, to account for any temperature variation between flow on/off conditions or any temperature gradients across the turret. The unsteady pressure and thermocouple data were acquired at 100 kHz for 10 seconds. The pressure-temperature data acquisition system was triggered simultaneously with the cameras, and all cameras' frames were acquired simultaneously with the pressure and thermocouple data.

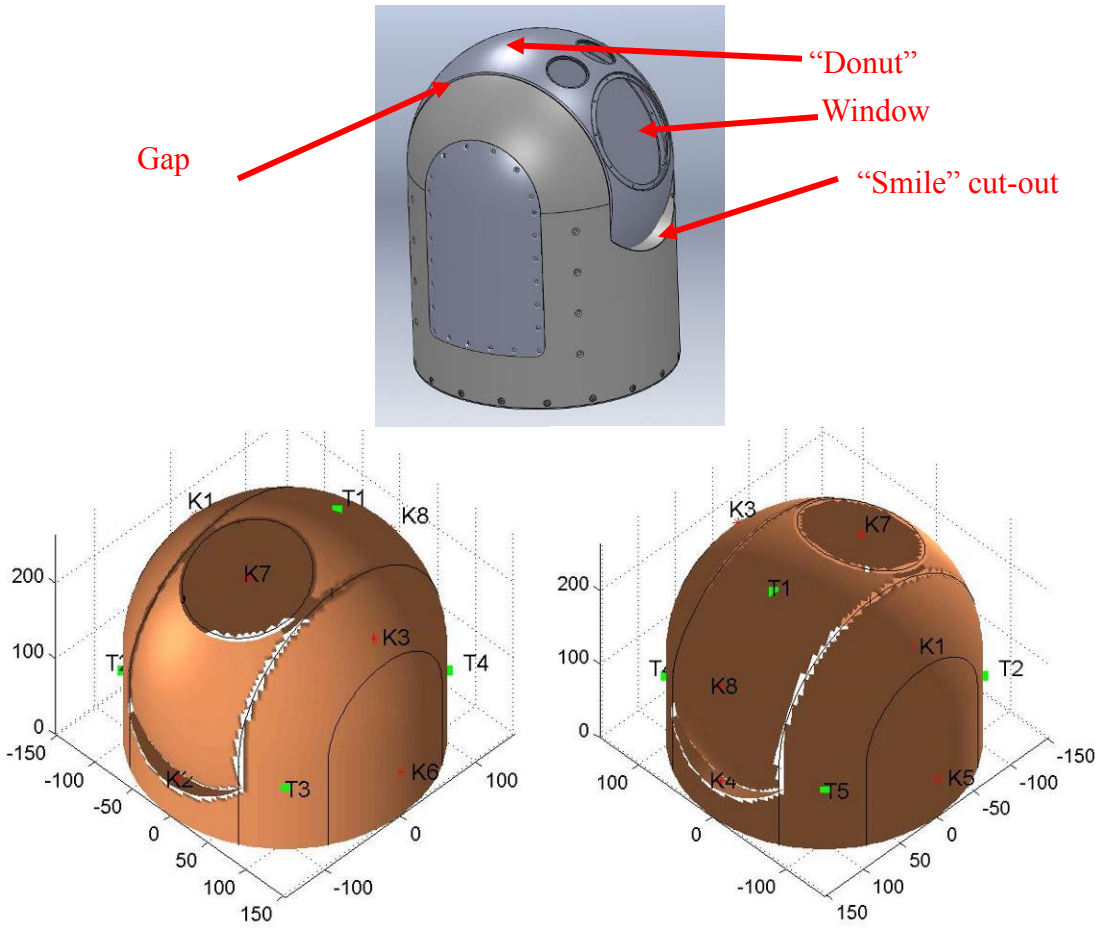

Figure 2. Top: Turret Model. Bottom: Locations of pressure sensors K1-K8 and thermoprobes, T1-T5, all dimensions are in mm.

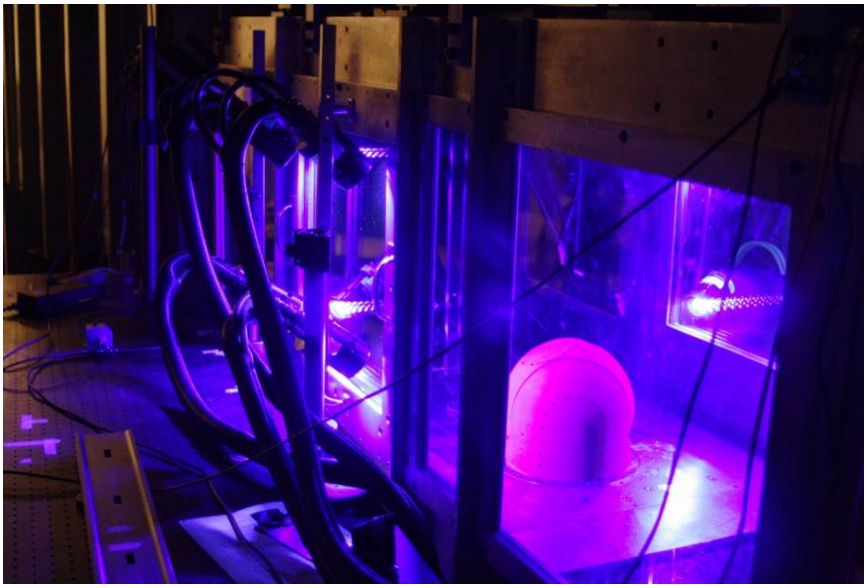

Figure 3. Turret model in the test facility.

Table 1: Camera properties.

	Camera 1	Camera 2	Camera 3
Colorspace	Greyscale	Greyscale	RGB
Resolution	1280 × 800	1024 × 768	1280 × 800
Frame Limit	5,477	7,000	7,000
Frames per Second	2,000	2,000	2,000

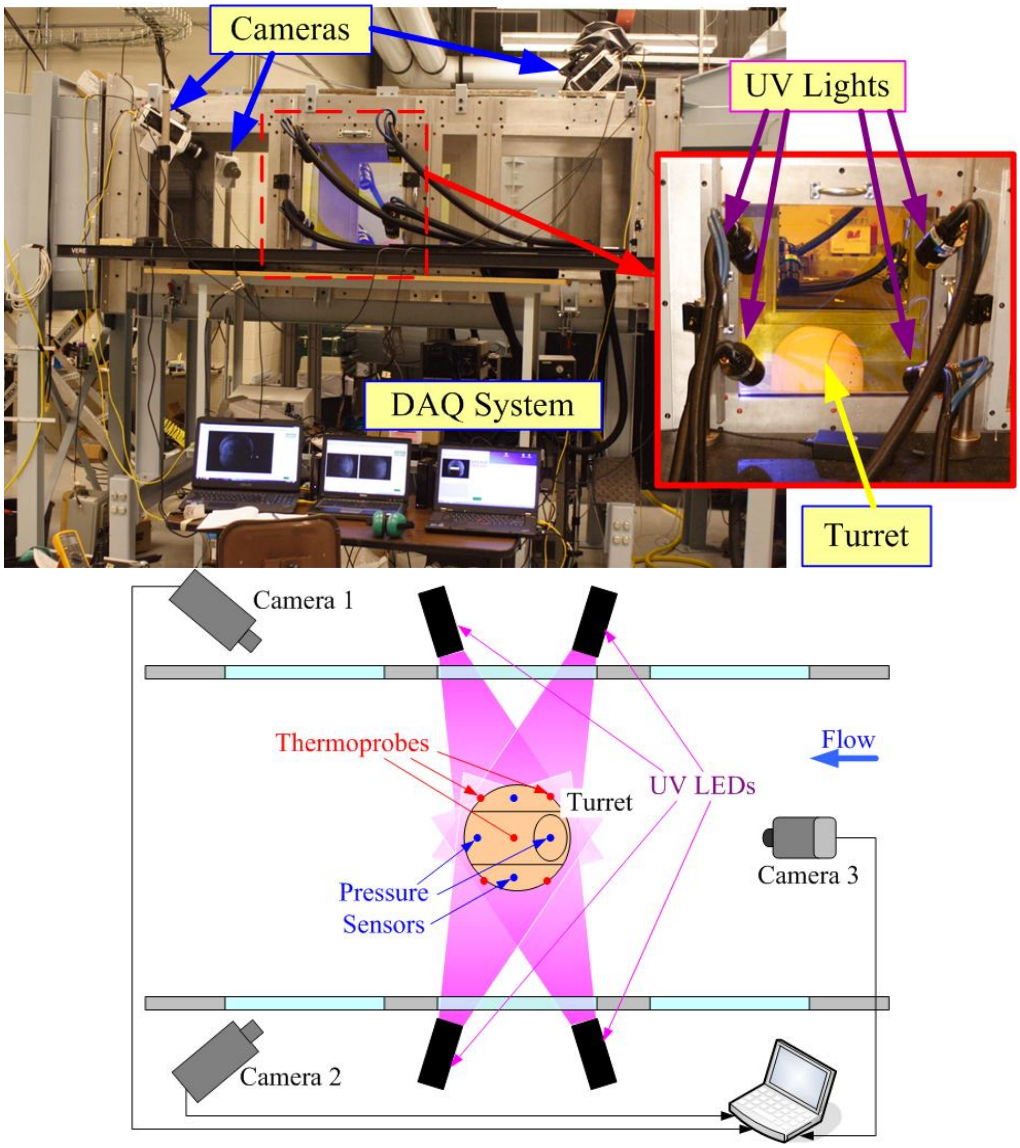

Figure 4. Hardware configuration: Picture (top) and schematic from the top view of wind tunnel. (bottom). Flow goes from right to left.

The turret geometric configurations tested are shown in Figure 5. It includes a test with a flat window, see Figure 5(a), and a test with a conformal window, shown in Figure 5(b). Additional tests were performed, in which the gaps surrounding the movable "donut" were covered with a metal tape, see Figure 5(c) and, finally, both gaps and 'smiles' were taped over, as shown in Figure 5(d), presenting the flow over a smooth surface rather than with various surface and surface slope discontinuities, caused by the presence of gaps and "smiles". Both the flat-window and the conformal-window turrets were tested at different azimuthal/elevation angles, indicated in Table 2. The azimuth angle was measured clockwise from the upstream direction, when viewed from above, and the elevation angle was measured upward from the horizontal plane.

Table 2: Test matrix of turret positions.

		Azimuth				
		0°	90°	125°	143°	180°
Elevation	45°	×*	×			× (flat only)
	60°				×	
	65°		×			
	69°			×		

* - for a conformal turret, included additional cases with gaps and "smiles" covered.

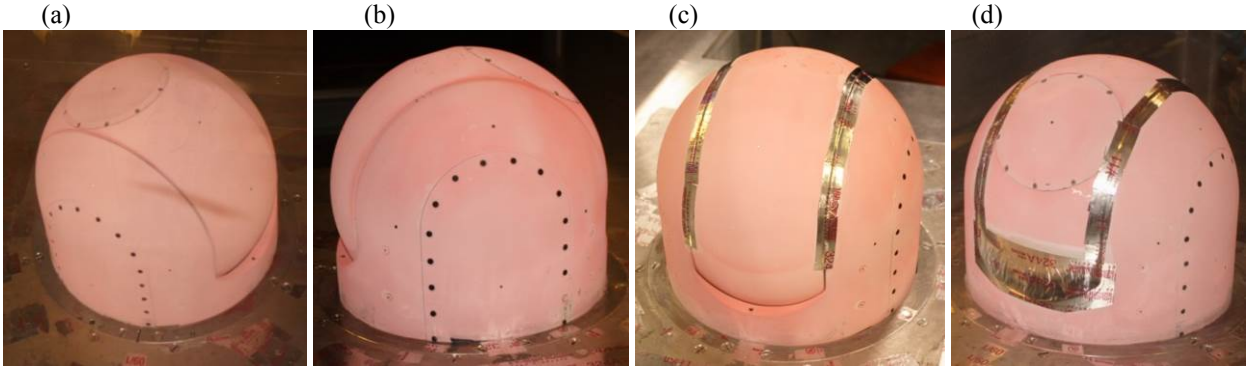

Figure 5. Different turret geometries tested during PSP tests: Turret with a flat-window (a), a conformal-window (b), a conformal-window with gaps covered (c) and a conformal-window with gaps and 'smiles' covered (d).

Data Reduction

PSP calibration

A calibration was performed using a painted coupon placed in a pressure- and temperature-controlled calibration chamber. At each of a specified series of conditions, an image of the coupon was made, and the conditions and average intensity recorded. Reference conditions were chosen to closely approximate those of the wind-off runs, and the pressure and intensity were normalized by these reference conditions. A surface fitting was used to provide a function returning a pressure ratio as a function of intensity ratio and instantaneous temperature.

This calibration was employed to extract instantaneous pressure fields from the registered images. The elementwise ratio of the flow-off mean to each flow-on frame was calculated, providing for each pixel a value of I_{ref}/I. Preliminary testing explored the possibility of using the average of the registered flow-on frames as the reference condition, but it was found that the change in temperature made this inaccurate for a reference condition. The advantage of using the flow-on reference as a reference is that bulk pressure shifts are cancelled out, isolating the temporal variations. To obtain this effect while maintaining the best fidelity to the data, a two-step procedure was implemented, where the flow-on mean was referenced directly to the flow-off mean, providing a base pressure ratio, i.e. $P_{ref_{on}}/P_{ref_{off}}$. The quotient of the instantaneous pressure ratio and the average pressure ratio provides a more accurate value of $P/P_{ref_{on}}$. Pressure fields were normalized by the dynamic pressure, $q = 0.5\rho U_\infty^2$. A complete description of the calibration procedure is given in [17].

Surface pressure reconstruction from PSP tests

Knowing exact location of each camera, relative to the turret, it is possible to map the pressure field from 2-D images onto the 3-D surface of the turret, using Perspective Transformation Matrix (PTM) technique [18,19]. The perspective projection is shown schematically in Figure 6.

The perspective transformation allows to compute (X_I,Y_I)-location of the image point, if a 3-D coordinate of the object point, (X_O,Y_O,Z_O), is given, as,

$$\begin{bmatrix} a \\ b \\ w \end{bmatrix} = PTM * \begin{bmatrix} X_O \\ Y_O \\ Z_O \\ 1 \end{bmatrix}, \quad X_I = a/w, \quad Y_I = b/w,$$

where *PTM* is the 3x4 Perspective Transformation Matrix, defined by the camera location and orientation angles. As accurate measurements of the camera orientation are difficult in practice, an alternative way to obtain PTM is to take images of several non-coplanar points with known 3-D coordinates. After extracting 2-D locations of the points from the image, TPM can be reconstructed using a least-square estimation [20]. The advantage of this method is that it does not require explicit knowledge of the camera' location and orientation.

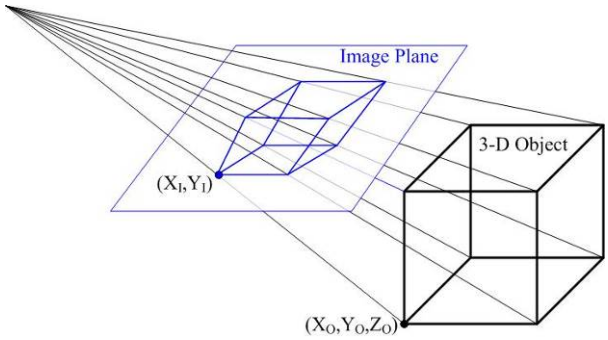

Figure 6. Schematic of perspective projection.

To accomplish this procedure, in the end of the PSP tests the turret was replaced with a calibration mask, consisted of a series of printed small dots at known locations. The mask was placed horizontally and then vertically and, for every case, images of the mask were recorded by all three cameras. After extracting 2-D locations of the dots from images, *PTM* was calculated for every camera.

The entire turret surface was approximated with a relatively dense grid, shown in Figure 7, middle plots. Then the turret surface was split into three regions to provide a unique mapping between the turret surface and the corresponding cameras' images. Using PTM for each camera, for every grid point on the surface of turret, a corresponding image point was calculated and, applying 10x10 Wiener filter centered at the image point, instantaneous pressure value at the point on the turret was found. After instantaneous pressure values at every grid point on the surface of the turret in each region were computed, the full surface pressure field was reconstructed, using weighing functions, shown in Figure 7, middle plots, to "blend" data from different cameras. An example of final 3-D reconstruction is shown in Figure 7, where individual 2-D pressure fields, shown in Figure 7, top row, were projected onto the 3-D turret surface, shown in Figure 7, bottom plot.

Cameras 1 and 2 were monochromatic and Camera 3 was color RGB. In order to capture different colors, the camera utilizes the Bayer arrangement of color filters on the pixel array of an image sensor, were each two-by-two cell contains two green, one blue, and one red filter. As an unintended consequence, the color camera measured colors on staggered grids with twice-less spatial resolution. A second issue with the color camera was that a combination of the staggered color grid and filters reduced an overall amount of intensity of the image, from 1000-2000 bits for the monochromatic camera down to 100-200 bits for the color camera. As image data are discrete both in space and bit values, this decrease in an overall intensity of the image resulted in an increased discretization error, up to 4-7% of the dynamic pressure, q, versus 0.7-1.5% of q for the monochromatic cameras. Camera 3 measured the region at the front portion of the turret, where pressure fluctuations, measured by unsteady pressure sensors, were found to be approximately 1-2% of the dynamic pressure. So the combination of much-less-intensity and lower-spatial resolution of the images made data acquired by the color Camera 3 very noisy, with very small signal-to-noise ratios. So, after various attempts to reduce noise present in images from Camera 3 by applying different filters, it was concluded that the signal-to-noise was very low and data from Camera 3 were ultimately excluded from the present analysis.

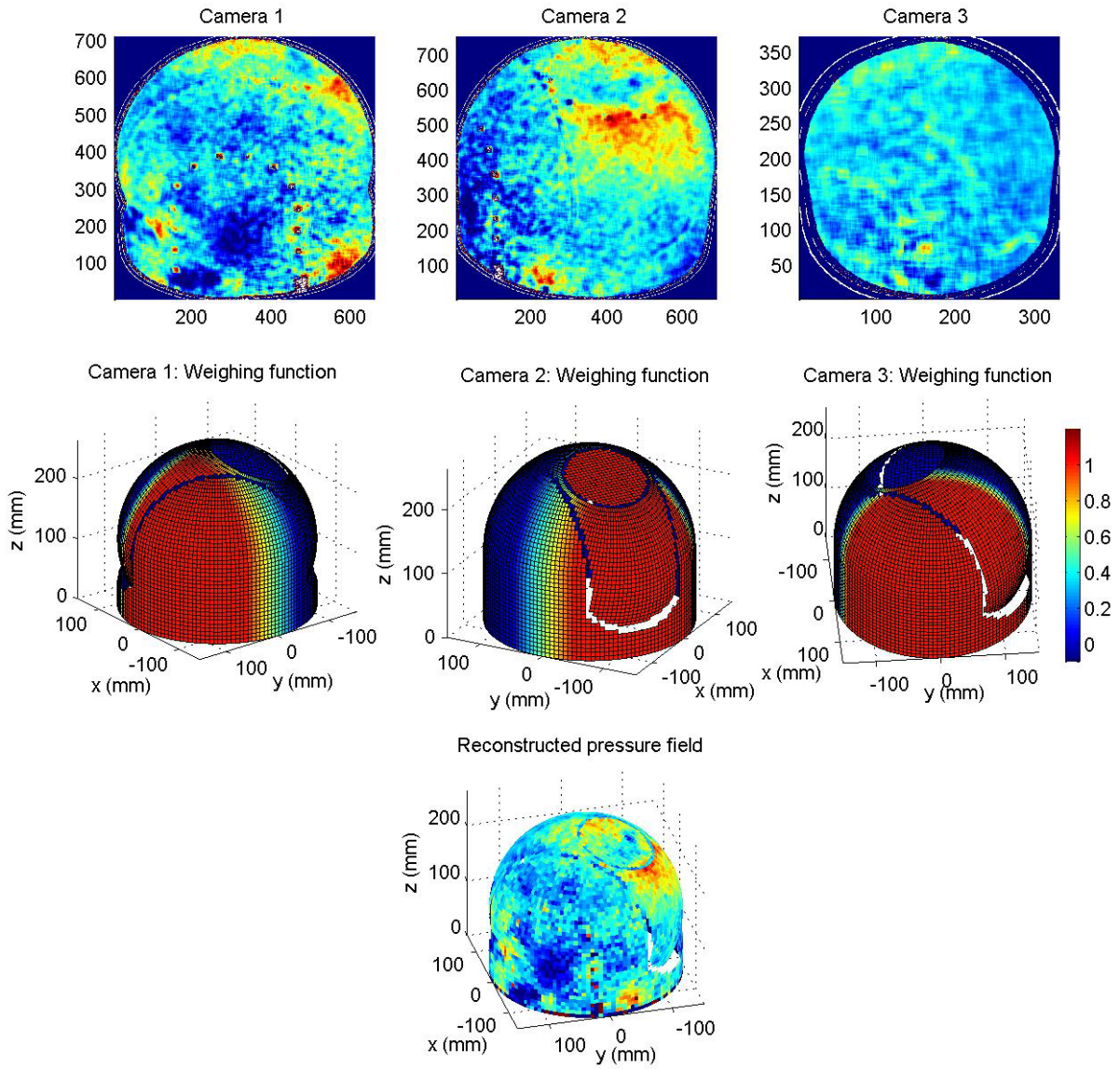

Figure 7: Top: Individual Frames from cameras. Middle: corresponding weighting functions. Bottom: reconstructed instantaneous pressure field on the surface of the turret. Flow goes along x-axis from positive to negative values.

POD analysis

To provide a framework to analyze and compare pressure fields for different turret configurations and window viewing angles, a Proper Orthogonal Decomposition (POD) was used [21]. From the spatially-temporally-resolved, mean-removed pressure field, $p(s,t)$, where s is the point of the turret, a time-averaged correlation matrix, $R(s,s') = \overline{p(s,t)p(s',t)}$, was calculated, where an overbar denotes a time averaging. Using the correlation matrix, a set of spatial POD modes, $\phi_n(s)$, and corresponding eigenvalues or mode energies, λ_n, can be found by solving an integral equation,

$$\int_S R(s,s')\varphi_n(s')ds' = \lambda_n \varphi_n(s) \tag{1}$$

The solution of Equation (1) gives a complete, orthogonal and fastest-converging set of POD modes. The instantaneous pressure field can be reconstructed using these modes as,

$$p(s,t) = \sum_n a_n(t)\varphi_n(s) \text{ , where } a_n(t) = \int_S p(s,t)\varphi_n(s)ds, \ \overline{a_n(t)a_m(t)} = \lambda_n \delta_{nm} \quad (2)$$

The fastest-converging property of POD technique allows approximating the instantaneous pressure field as a sum of first N modes, $p(s,t) \approx \sum_n^N a_n(t)\varphi_n(s)$.

Equations (1) and (2) were discretized over the turret grid and numerically solved using Matlab for every measured angle and a geometry type. Also, the normalized mode energy, $\lambda_n \equiv \lambda_n / \sum_n \lambda_n$, and the normalized cumulative energy, $\sigma_m \equiv \sum_n^m \lambda_n / \sum_n \lambda_n$, were computed for each case.

Figure 8 presents both the normalized and cumulative energies for the (90,45), flat-window case. Here and below the viewing angle is given in parenthesis with the azimuthal angle as the first number and the elevation angle as the second number. The full POD set for this case had more 4000 modes, but the first POD mode contained almost 30% of the total energy of the pressure fluctuations, first 10 modes have more than 60% of the energy, first 100 modes held more than 80% of the total pressure-fluctuating energy and 3000 modes captured virtually all pressure "energy" of the flow.

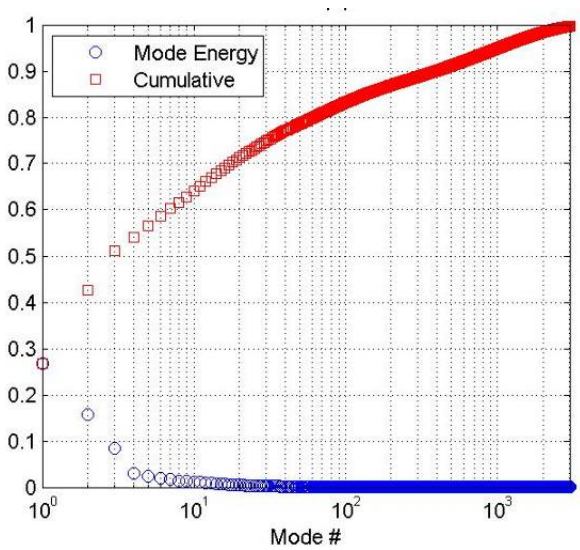

Figure 8. The normalized and cumulative mode energies for (90,45)-Flat case.

To further illustrate the converging property of the POD set, the pressure field for the same case at a given moment was reconstructed using first 10, 100 and 1000 POD modes and results are presented in Figure 9. The original pressure field is also presented in Figure 9, top left. As few as 10 POD modes were able to capture most of the essential pressure features and all of the features were properly recovered using 100 modes. The addition of more modes simply added more noise to the pressure field, as the POD technique arranged modes by amount of cross-correlation or "order", so mostly incoherent noise was present in very high-order modes. Thus, the POD technique, in addition to providing an optimal framework to investigate the flow, also presents an efficient way to remove the noise present in the experimental data, while preserving structures' features. After analyzing all cases, it was decided to keep only first $N = 100$ modes in POD-based pressure reconstruction for the reminder of the paper.

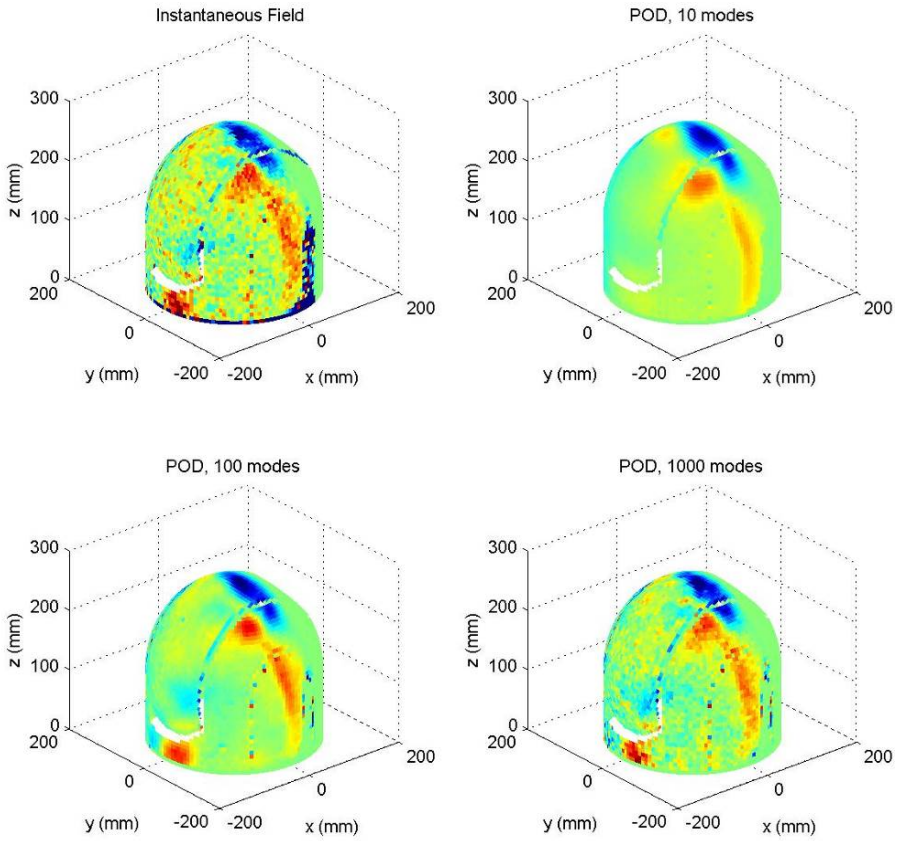

Figure 9. The representative instantaneous pressure field (top left) and POD reconstruction using 10 (top right), 100 (bottom left) and 1000 (bottom right) POD modes. (90,45), flat-window case, the flow goes along x-axis from positive to negative values.

Results

Comparison between PSP and unsteady pressure sensors

Figure 10 presents a comparison between pressure spectra from unsteady pressure sensors and pressures extracted from PSP tests at three different locations of the turret. There is a very good agreement in both magnitude and frequency content between the pressure spectra, except for the very end of the PSP-spectrum, where PSP-spectra leveled off due to bit resolution errors and possibly an insufficient sampling rate. Thus, using PSP-technique, the pressure field over the turret surface was properly resolved in both time and space.

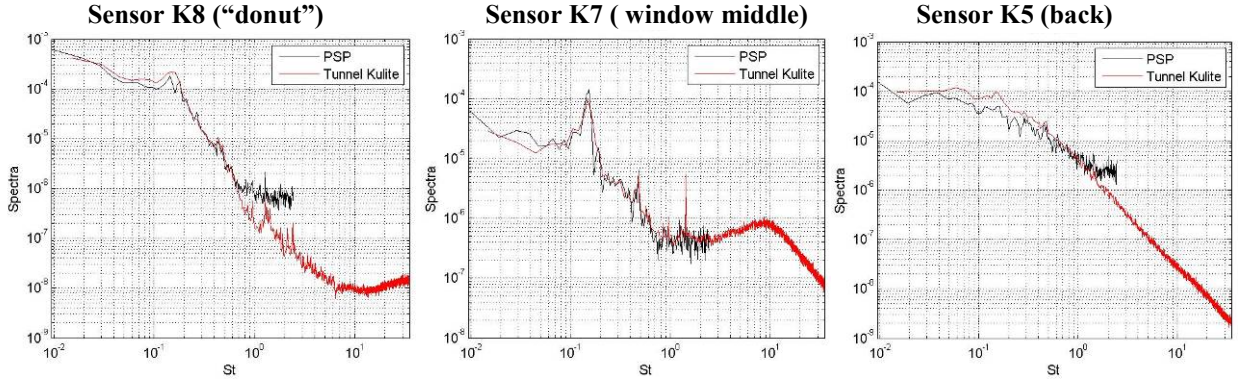

Figure 10. Pressure amplitude spectra from unsteady pressure sensors (Kulites) and PSP for three different locations for (90,45), flat-window turret.

Effect of turret geometry and azimuthal/elevation angle

Maps of time-averaged spatial $p_{rms}(s)$ for different azimuthal/elevation angles for the conformal-window turret are presented Figure 11. A dark blue color at the front portion of the turret in Figure 11 and in Figures 14 and 24 corresponds to a no-data region corresponding to Camera 3; no-data were replaced with zeros for illustrative purposes only and were not included in POD analysis. The moving flow separation off the turret's backward surface caused the temporal pressure fluctuations just upstream of the separation line, labeled in Figure 11. Another region of increased pressure fluctuations was near the bottom of the downstream portion of the turret; this increase was due to an unsteady stagnation region caused by the recirculating flow region downstream of the turret, as well as a pair of "horn" vortices, located on both sides of the stagnation region, see Figure 1.

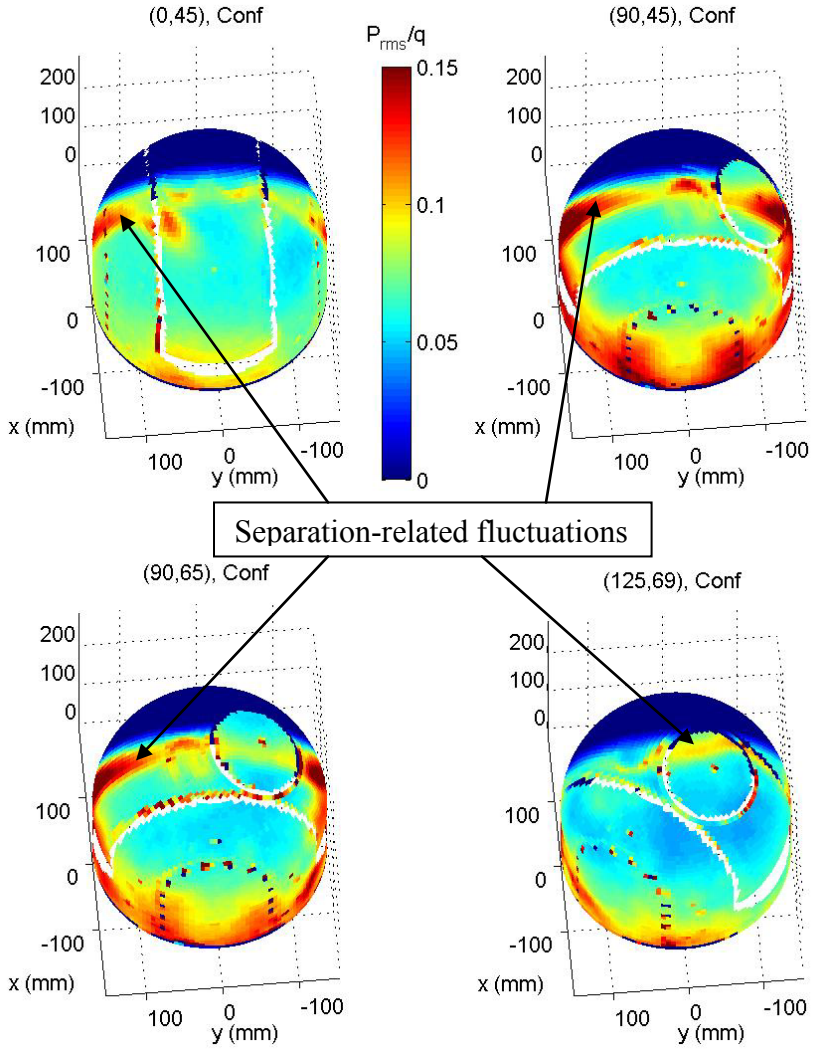

Figure 11. Spatial distributions of $p_{rms}(s)$ for different window azimuthal/elevation angles for the conformal-window turret. The flow goes along x-axis from positive to negative values. Z-axis is not labeled for clarity.

Clearly, the spatial intensity of the pressure fluctuations depended on the location of gaps and "smiles", relative to the flow direction. When "smiles" were located at the front and at the aft of the turret, they did not significantly effect of the flow around the turret, see Figure 11, upper left plot. Then the turret was rotated by 90 degrees, so the "smiles" were positioned spanwise-symmetrically on both sides of the turret. Slope discontinuities around "smiles", particularly upstream vertical back-steps, tripped the flow, so the flow separated prematurely on both sides of the turret and created strong vortical structures, clearly visible in a representative instantaneous pressure fields in Figure 12; these structures, through an interaction with the main separated region significantly increased pressure fluctuations near the bottom of the turret, see Figure 11, upper right and bottom left plots. When the "smiles" were

positioned non-symmetrically in the spanwise direction, for the (125,69)-case, for instance, they introduced spanwise-asymmetric spatial pressure fluctuations, see Figure 11, bottom right plot. Inspection of the instantaneous pressure fields, shown in Figure 13, revealed that the upstream "smile" created strong vortical structures, while no significant structures were formed by the downstream "smile". Also, for this azimuthal angle, the vortical structures were located closer to the mounting wall, compared to the azimuthal angle of 90 degrees, suggesting that the curved, cavity-like portion of the "smile" was primarily responsible for creating vortical structures.

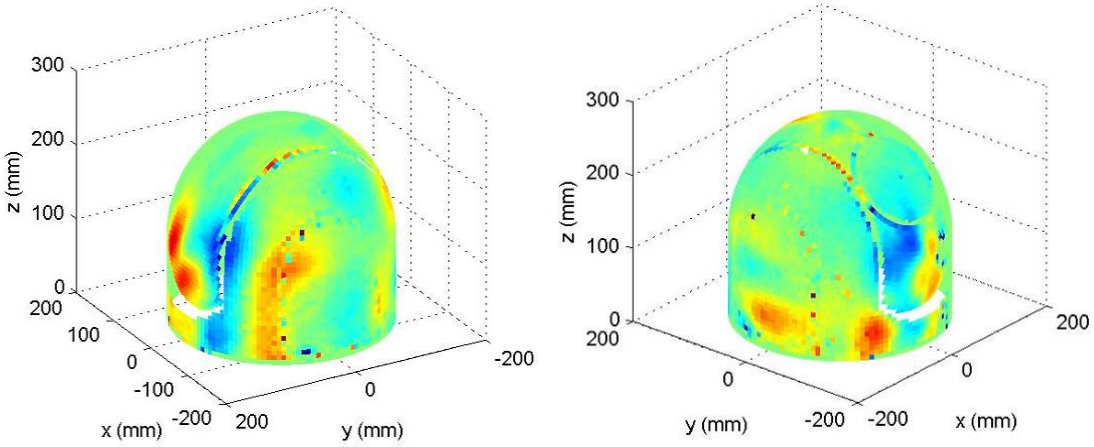

Figure 12. Representative instantaneous pressure fields for (90,45), conformal-window case. The flow goes along x-axis from positive to negative values.

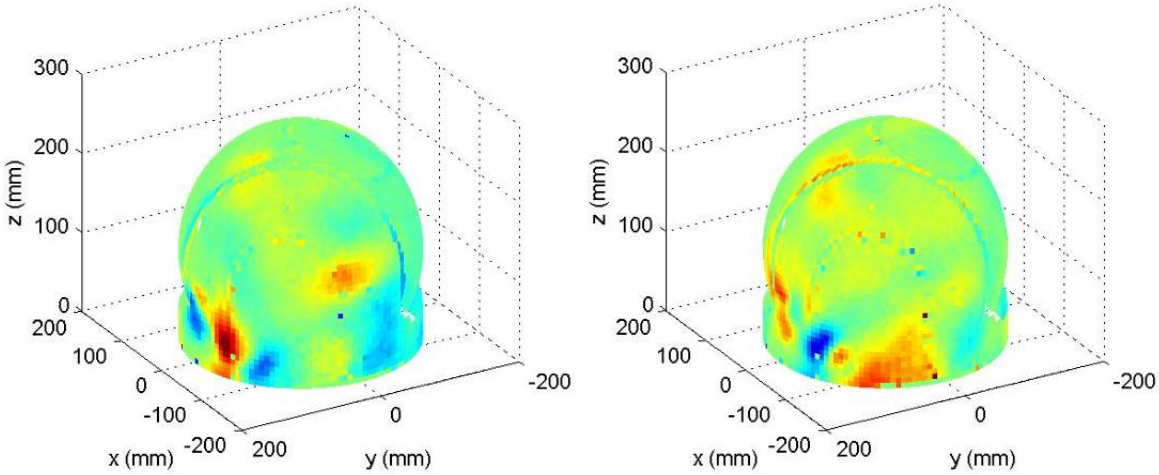

Figure 13. Representative instantaneous pressure fields for (125,69), conformal-window case. The flow goes along x-axis from positive to negative values.

Spatial distributions of the pressure fluctuations, $p_{\mathrm{rms}}(s)$, for the same angles, but for the flat-window turret are shown in Figure 14. When the flat-window was facing forward, the slope discontinuity around the window tripped the flow and created vortical structures which convected over the top of the turret, shown in representative instantaneous pressure fields in Figure 15; they were responsible for an additional increase in pressure fluctuations on top of the turret, see Figure, 14, upper left plot, compared to the conformal-window turret for the same viewing angle, shown in Figure 11, upper left plot. For side-looking angles of (90,45), (90,65) and (125,69), see Figure 14, corresponding plots, the presence of the flat window created only small deviations from the spatial pressure fluctuations for the conformal-window turret for the same angles, see Figure 11, corresponding plots. Predictably, most of the changes occurred over the flat-window aperture, where it created a slightly-different pressure gradient and locally chanced the flow dynamics and topology. A most notable difference for the pressure field over the window was observed for (125,69) and (143,60) cases, where a slow-moving time-changing local vortex was observed at the bottom of the flat window, creating a local increase in the pressure fluctuations, labeled in Figure 14, bottom left and middle plots. Nevertheless, overall spatial distributions of temporal pressure fluctuations were found to be more sensitive to the positions of the "smiles", rather than to the window type or its location. When the turret

was rotated to the azimuthal angle of 143 degrees, the upstream "smile" was in the region of the strong favorable pressure gradient at the upstream portion of the turret, so the tripped-by-"smile" flow quickly reattached and the formation of the vortical structures on that side of the turret was greatly suppressed, see representative snapshots of the pressure field in Figure 16.

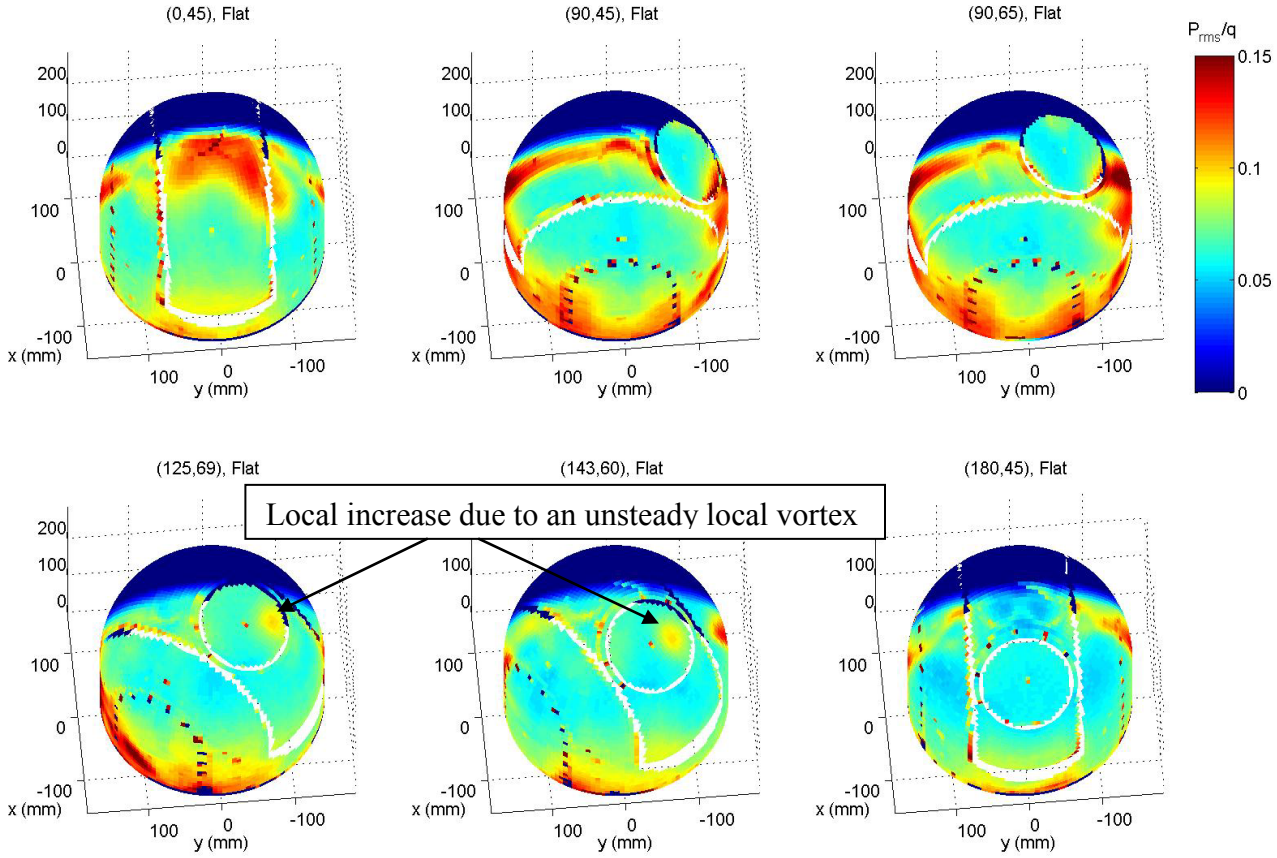

Figure 14. Spatial distributions of $p_{rms}(s)$ for different window azimuthal/elevation angles for the flat-window turret. The flow goes along x-axis from positive to negative values. Z-axis is not labeled for clarity.

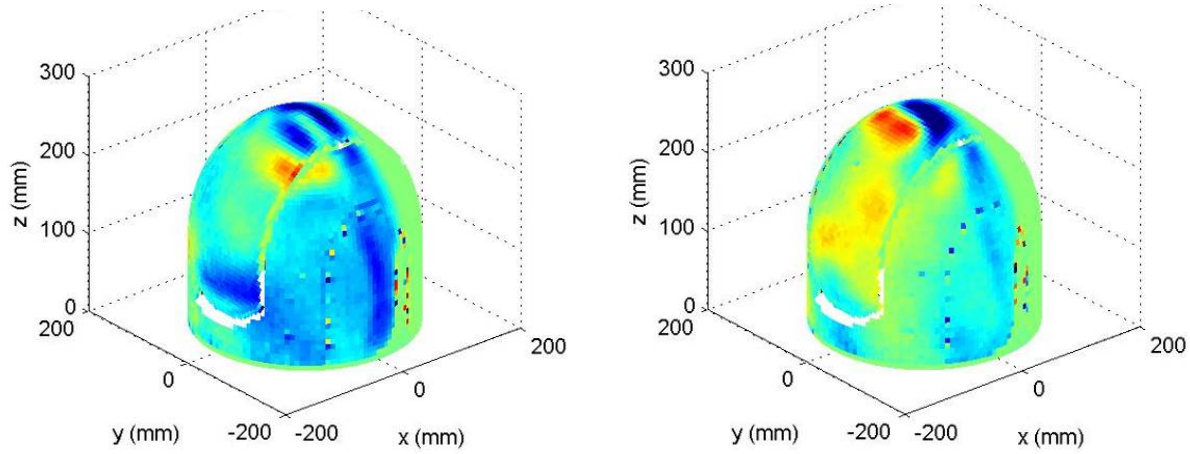

Figure 15. Representative instantaneous pressure fields for (0,45), flat-window case. The flow goes along x-axis from positive to negative values.

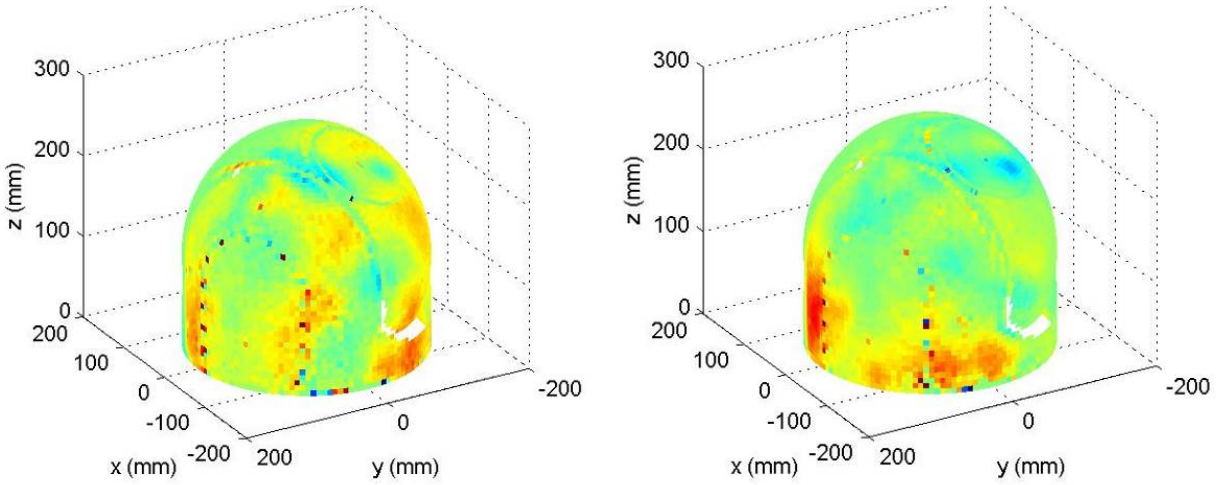

Figure 16. Representative instantaneous pressure fields for (143,60), flat-window case. The flow goes along x-axis from positive to negative values.

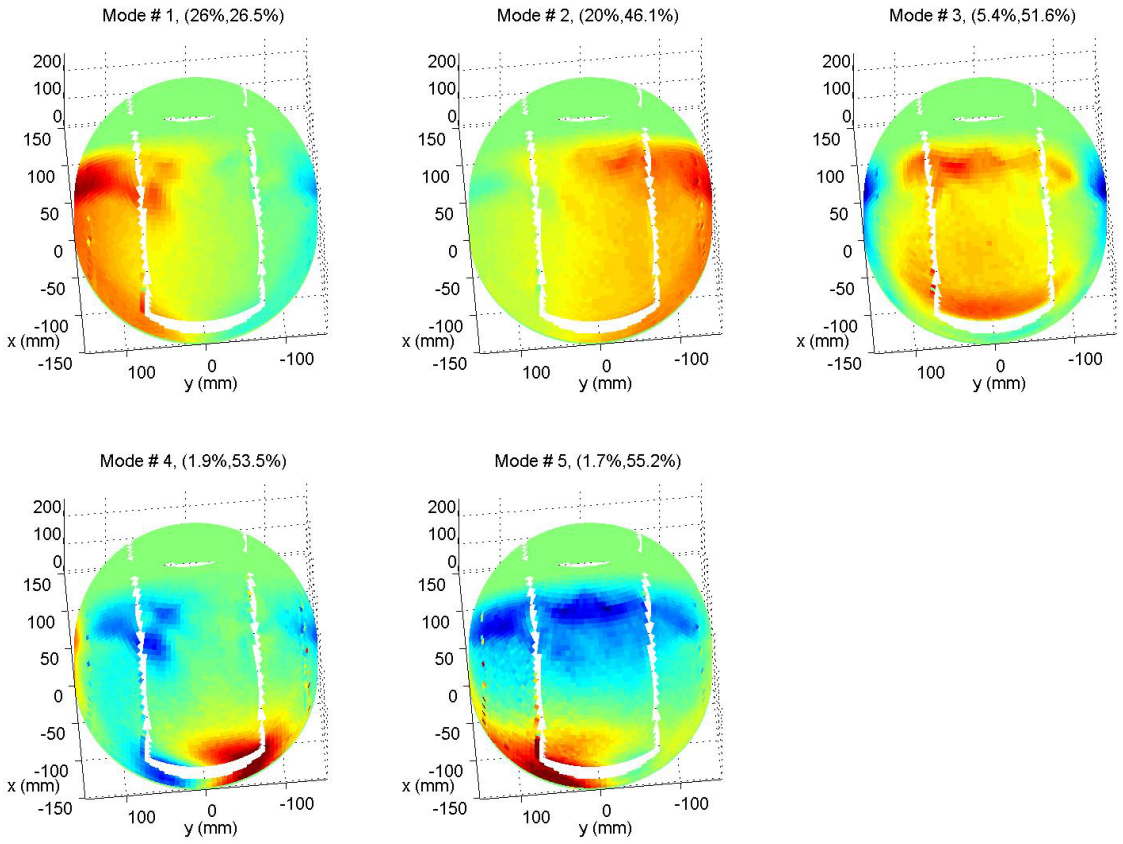

Figure 17. First 5 POD modes for the (0,45)-case for the conformal-window turret. The flow goes along x-axis from positive to negative values. Z-axis is not labeled for clarity.

POD modes and the corresponding temporal coefficients, as well as normalized and cumulative energies were calculated for every case. First five dominant modes for (0,45)-case for both the conformal- and the flat-window geometries are presented in Figure 17 and Figure 18, respectively; the corresponding normalized and the cumulative energies for each POD mode are given as a first and a second numbers in parenthesis on top of every plot and all other plots of POD modes in this paper. For the conformal geometry, Figure 17, the first two POD modes had 26% and 20% of the total pressure energy and spatial distributions of these modes reveal that they corresponded to the

separation-line-related pressure fluctuations, already discussed in Figure 11. Thus, the separation-related pressure fluctuations were a dominant source of the overall pressure fluctuations on the surface of the turret. These two modes appeared to be almost mirror images of each other relative to the vertical streamwise centerplane and had essentially non-zero values only at one side of the turret; as POD modes are statistically-uncorrelated, this suggested that the separation-related pressure fluctuations on either side of the turret were statistically-independent. The third mode was also related to the different region of the separation line located primarily on top of the turret; it appeared to be symmetric relative to the vertical streamwise centerplane. Modes 4 and 5 were related to the unsteady stagnation region at the bottom of the turret, caused by the recirculating flow downstream of the turret. Analysis of higher modes (not shown) had revealed that they described additional details of the dynamics of the separation line and the stagnation region.

Five dominant POD modes for the same window viewing angle of (0,45), but for the flat-window turret are presented in Figure 18. The first two modes were similar in spatial distribution, as for the first two POD modes for the conformal-winnow turret, shown in Figure 17, two left upper plots, except for the region on top of the turret, where the separation was disturbed by additional vortical structures created by the premature separation over the facing-forward flat-window aperture, see Figure 15; also for the flat-window geometry the first mode had only 22% of the total energy and the second had only 12% of the total energy. Modes 3-5 were related to the vortical structures convecting over the top of the flat-window turret. Overall, due to more interaction between the main separated region downstream of the turret and additional vortical structures introduced locally by the flat window, the flow over the flat-window turret was less "organized", as it took first 6 modes to capture 50% of the total pressure energy, compared to the conformal-window turret, where 50% of the energy were contained in first 3 modes.

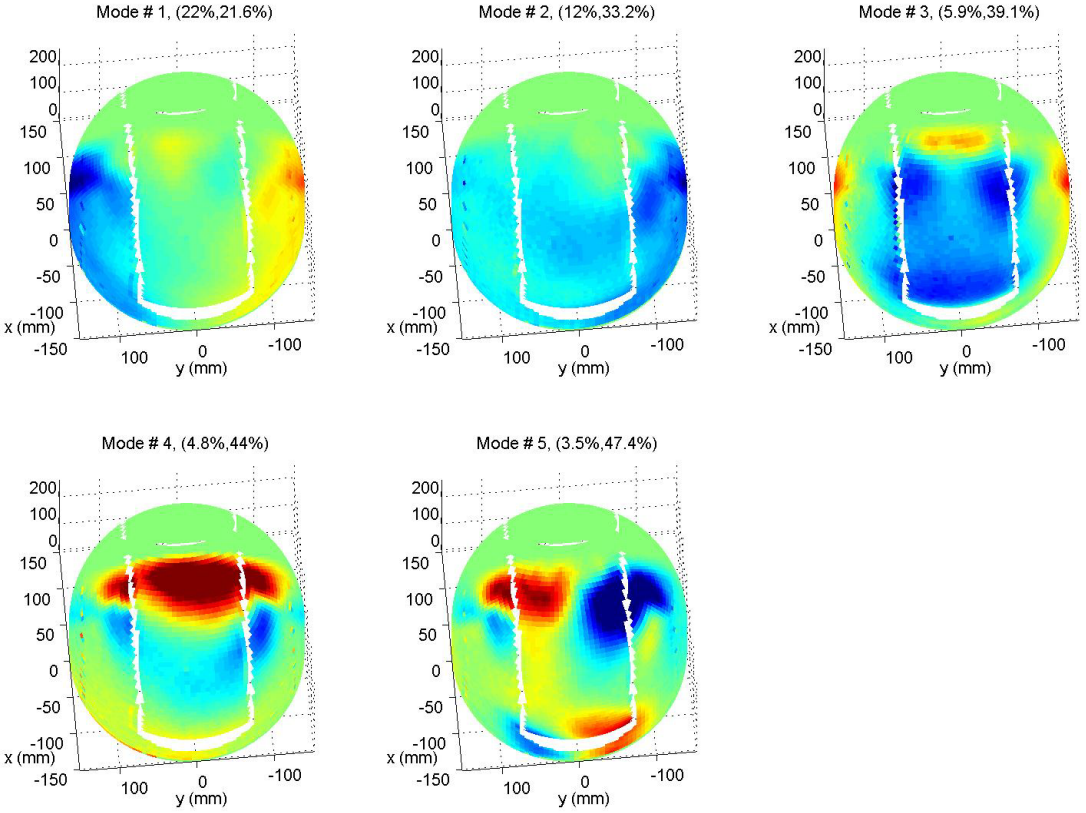

Figure 18. First 5 POD modes for the (0,45)-case for the flat-window turret. The flow goes along x-axis from positive to negative values. Z-axis is not labeled for clarity.

Power spectra of the temporal coefficients of the dominant five POD modes for the conformal- and the flat-window turret are presented in Figure 19, left and right plots, respectively. For both window geometries, first two modes had a peak around $St_D = 0.2$ and a smaller, sharper peak around $St_D = 0.5$. The first peak was related to the unsteady flow separation over the turret; similar values of the unsteady-pressure spectral peak were observed in

other unsteady pressure measurements on the downstream portion of the turret [22, 23]. The origin of the second peak was not quite clear and possibly was related to the blade passing frequency of the tunnel-driving fan.

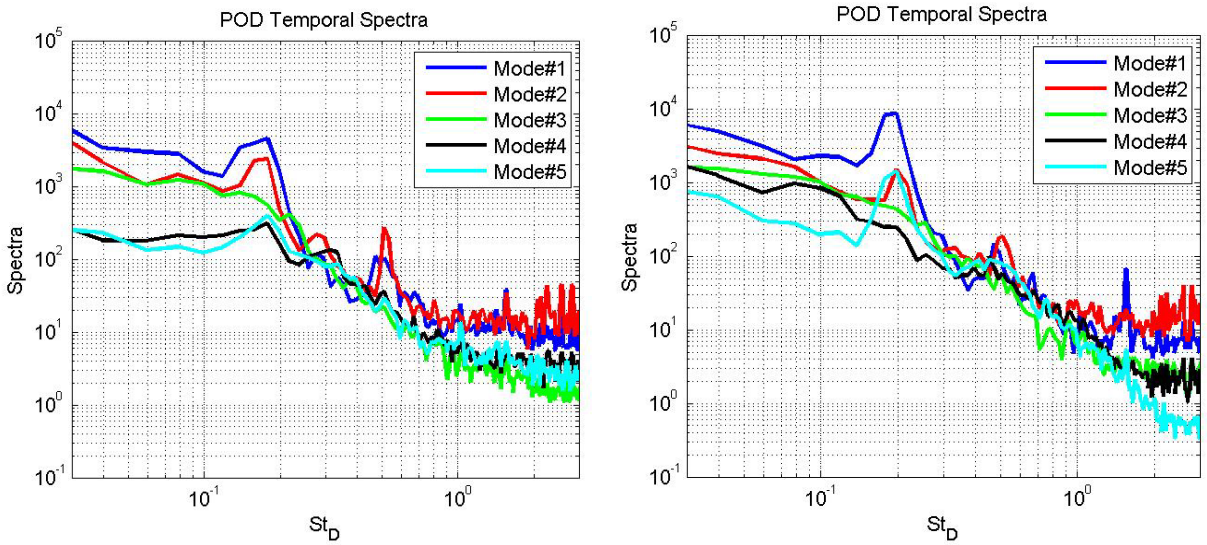

Figure 19. Spectra for temporal coefficients for first 5 POD modes for the (0,45)-case for the conformal (left plot) and flat-window (right plot) turrets.

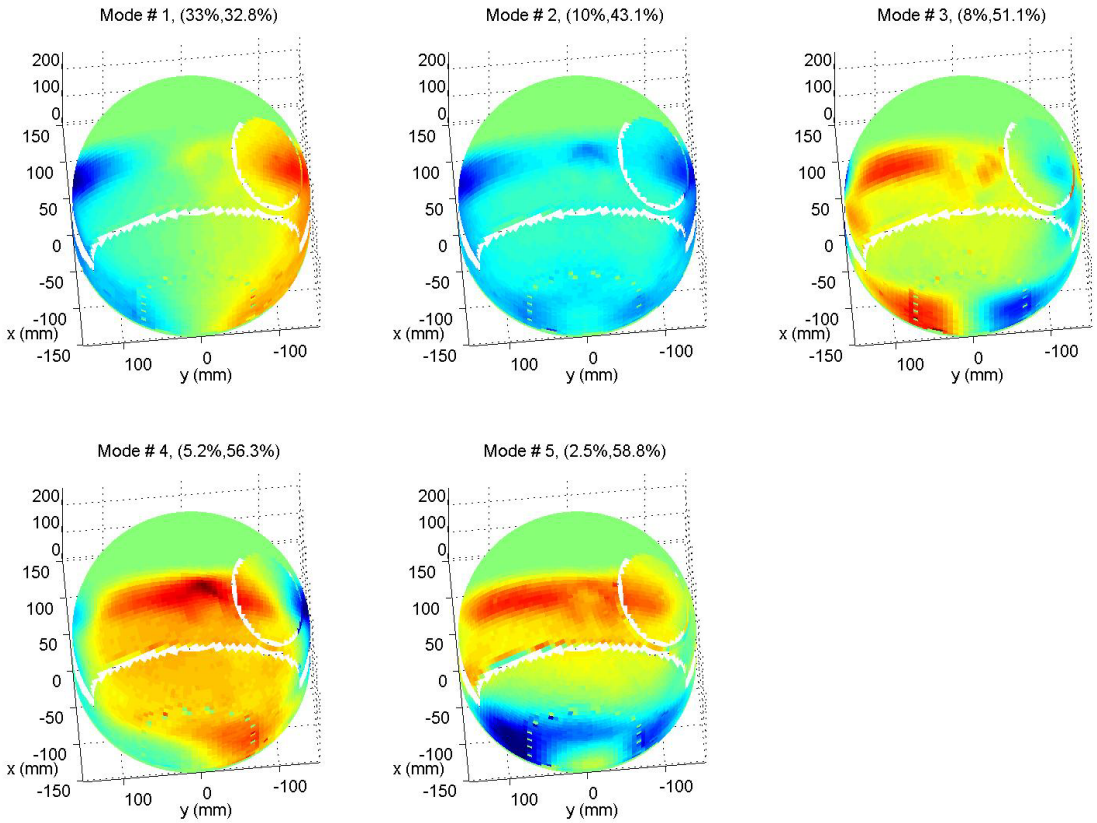

Figure 20. First 5 POD modes for the (90,45)-case for the conformal-window turret. The flow goes along x-axis from positive to negative values. Z-axis is not labeled for clarity.

When the turret was rotated to the window azimuth angle of 90 degrees, both "smiles" were positioned symmetrically on each side of the turret, relative to the incoming flow. In Figure 12 it was demonstrated that the

prematurely-forced flow separations were caused by the "smile" slope discontinuities and were responsible for a significant increase of the pressure fluctuations downstream of "smiles"; thus, dominant POD modes for (90,45), conformal-window case, shown in Figure 20, were significantly different from the POD modes for the conformal-window turret for (0,45)-case. The first mode had a 33% of the total pressure energy and its spatial distribution was spanwise anti-symmetric, suggesting that the separation-related pressure fluctuations on both sides of the turret were strongly correlated and out-of-phase; recall that separation-related modes 1 and 2 for the (0,45)-case were largely uncorrelated. POD modes 3-5 were related to the unsteady stagnation region downstream of the turret.

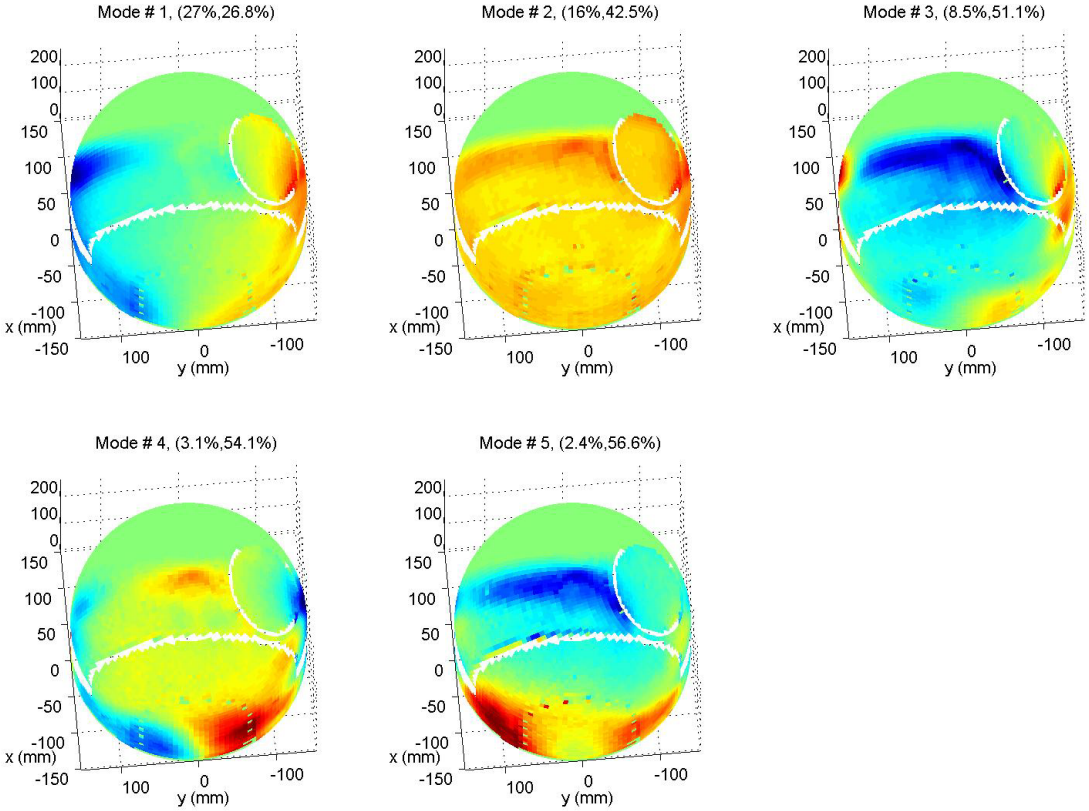

Figure 21. First 5 POD modes for the (90,45)-case for the flat-window turret. The flow goes along x-axis from positive to negative values. Z-axis is not labeled for clarity.

Dominant POD modes for the flat-window turret and the same (90,45)-viewing angle are presented in Figure 21. While the side-facing flat-window did introduce an asymmetry to the turret surface, POD modes were similar to the modes for the conformal-window turret (although not necessarily in one-to-one comparison, as Mode 3, conformal was similar to Mode 4, flat), confirming that the dominant sources of pressure fluctuations were "smiles". Spectra of the temporal coefficients for dominant POD modes were quite similar to the spectra for (0,45)-case, shown in Figure 19, with a dominant peak around $St_D = 0.2$ and therefore are not presented here.

Analysis of higher-order modes revealed statistical details about less-energetic, but still dynamically-important features, like "smile"-induced traveling vortical structures observed for viewing angles of (90,45), see Figure 12, and for (125,69), shown in Figure 13. For (90,45)-case, Modes 5-8, presented in Figure 22, left plots, showed the streamwise spacing of approximately 45 degrees between positive and negative values in POD modes downstream of the "smiles", which is related to the average streamwise spacing between traveling structures. Also, POD modes showed a significant extent of the traveling structures away from the mounting wall, up to a more than a half of the total turret height. In comparison, for (125,69)-case, shown in Figure 22, right plots, traveling structures were located closer to the wall, mostly on the cylindrical portion of the turret, with very similar spacing between structures. So, the details of the instantaneous pressure fields were sensitive to the relative positions of "smiles".

While traveling vortical structure had well-defined spatial spacing between consecutive structures, the analysis of the spectra of temporal coefficients for Modes 5-8 for (90,45) and (125,69) , shown in Figure 23, did not reveal any clear periodicity, except for a very small peak around $St_D = 0.2$. This suggests that the structures at these viewing angles were shed off of the "smiles" randomly.

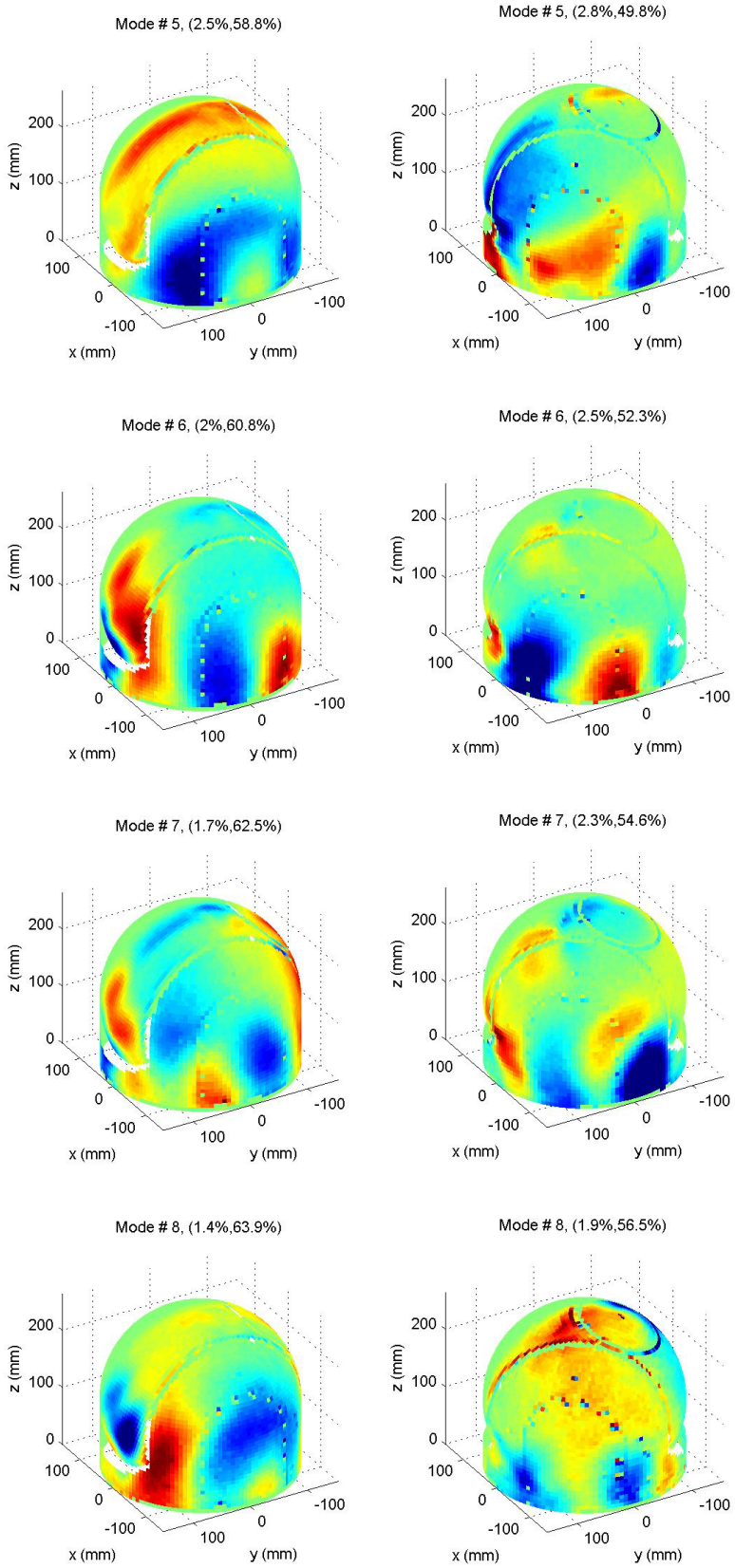

Figure 22. POD modes 5-8 for the conformal turret for the (90,45)-case (left plots) and for (125,69)-case (right plots). The flow goes along x-axis from positive to negative values.

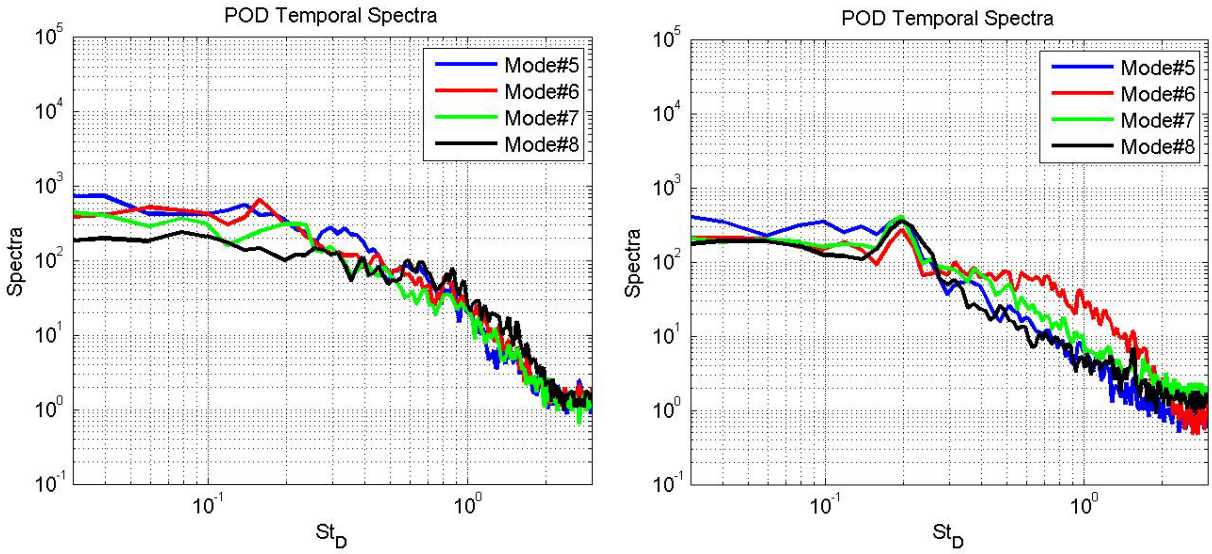

Figure 23. Spectra for temporal coefficients for higher POD modes #5-8 for the (90,45)-case (left plot) and for (125,69)-case (right plot) for the conformal-window turret.

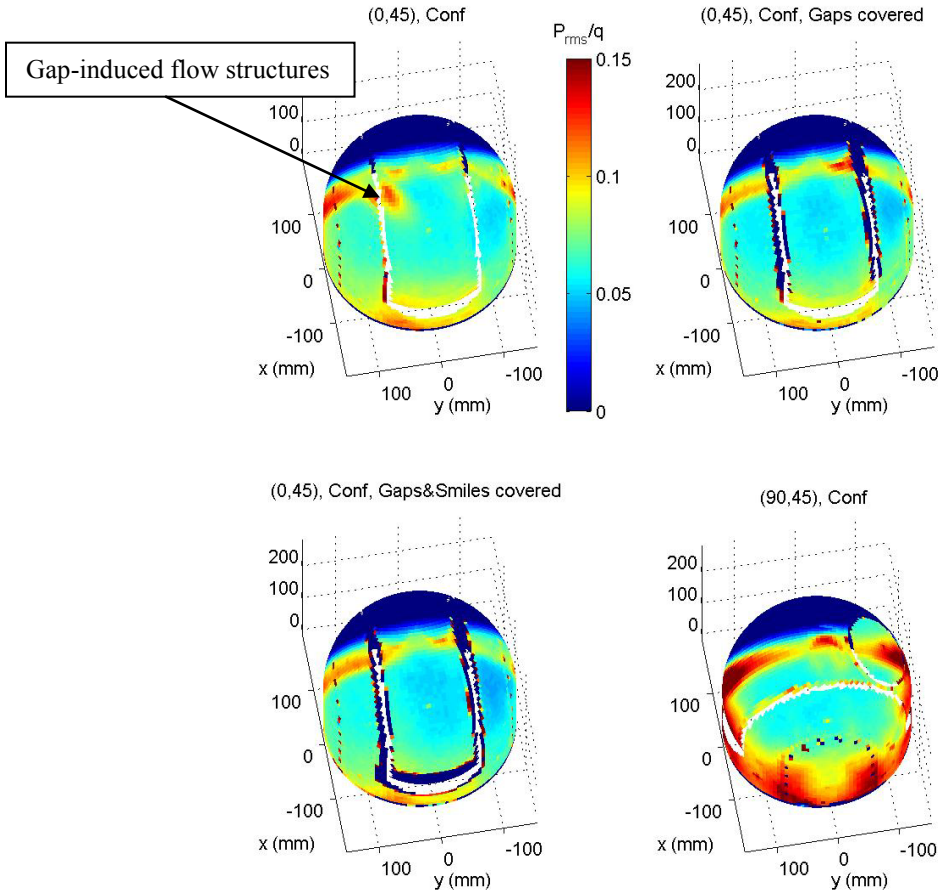

Figure 24. Spatial distributions of $p_{\mathrm{rms}}(s)$ for the conformal-window turret at (0,45) for (a) gaps open, (b) gaps covered, (c), gaps and "smiles" covered and (d) at (90,45) with gaps and smiles" uncovered. The flow goes along x-axis from positive to negative values. Z-axis is not labeled for clarity.

Effect of the presence of gaps and "smiles"

By covering gaps and "smiles" one can directly study their effects on the instantaneous pressure field. Time-averaged spatial distribution of the unsteady pressure fields for (0,45), conformal-window case are presented in Figure 24, with both gaps and smiles present, gaps covered and both gaps and "smiles" covered. For this azimuthal angle, gaps were aligned with the incoming flow and air was forced to flow through gaps due to pressure gradients on the surface of the turret. The flow through gaps formed weak blowing jets on the downstream portion of the turret. The interaction of jets with the separated flow created additional vortical structures, which were responsible for a localized increase in p_{rms}-values, marked in Figure 24, top left. Representative instantaneous pressure fields for gaps uncovered, highlighting these structures, are shown in Figure 25. At this window viewing angle of (0,45), the "smiles" were located either at the front or at the back of the turret and did not significantly disturb the flow. As a result, there was no difference between the covered-gaps geometry and the covered-gaps-and-smiles geometry, see Figure 24. But when "smiles" were positioned at the azimuthal angle of +-90 degrees, as for (90,45) case, the smile-related slope discontinuities tripped the flow prematurely and significantly increased levels of p_{rms} on the downstream portion of the turret, as already discussed in detail above, see Figure 24, bottom right.

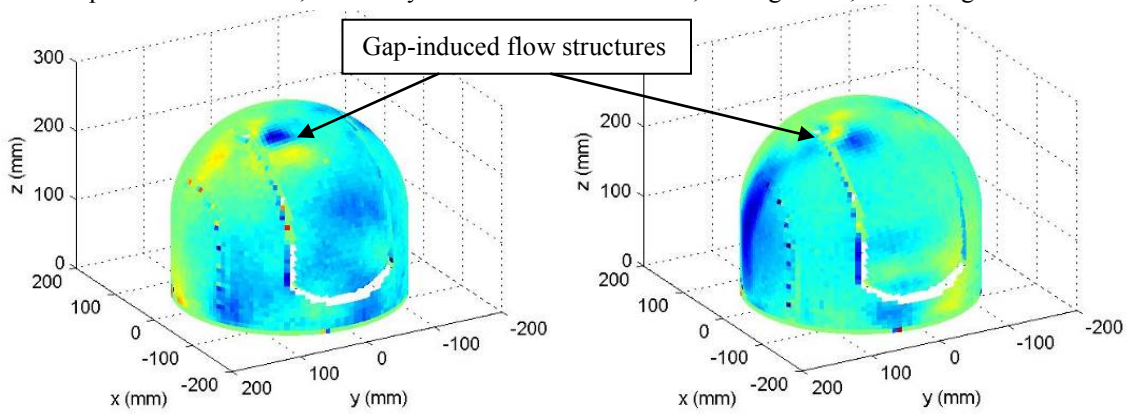

Figure 25. Representative instantaneous pressure fields for (0,45), conformal-window case with gaps and "smiles" present. The flow goes along x-axis from positive to negative values.

Joint POD analysis

While POD finds an optimal set of eigenmodes for every data set and it is useful to examine each POD set separately, it gives a *different* set for every case. In order to perform a proper comparison between different cases to examine, for example, the effect of either the flat or the conformal window on the pressure field, one can combine data sets for both cases and find the *joint* POD spatial set, which, by construction, will be the same for both cases and the difference will be only in temporal coefficients and, consequently, in values of normalized and cumulative energies.

An example of the joint POD analysis for (0,45) viewing angle is shown in Figure 26, where fist nine joint POD modes are presented for a combined dataset including both the conformal- and the flat-window cases. As before, first three dominant modes were related to the unsteady flow separation off the surface of the turret, and the other modes described the vortical structures formed by the facing-forward flat window. To study the contribution of each mode to the unsteady pressure field as a function of geometry, each joint POD mode was projected into the instantaneous pressure field corresponding to the conformal-window turret and, separately, to the flat-window turret to compute temporal coefficients. Time-averaged squares of the temporal coefficients of each joint mode for different geometries, which are relative energies of each mode, are presented in Figure 27, left, and the normalized cumulative energies for each geometry are plotted in Figure 27, right. For the conformal-window turret, the first two joint POD modes were more energetic than the for the flat-window turret, indicating that the flat-window-induced separation disrupted the overall separation over the turret. Modes 4-20 were more energetic for the flat-window turret, compared to the conformal-window turret, as these modes described the details of the flat-window-induced separation on top of the turret, and the conformal-window turret did not have this separation. First 100 joint POD modes described 80% of the total pressure energy, very similar for first 100 POD modes from individual POD sets. Thus, the joint POD approach allows studying the relative contribution of each joint POD mode to the pressure dynamics for particular turret geometry. Similarly, the approach can be used to study the relative importance of each joint POD mode as a function of the window viewing angle by combining datasets for these angles.

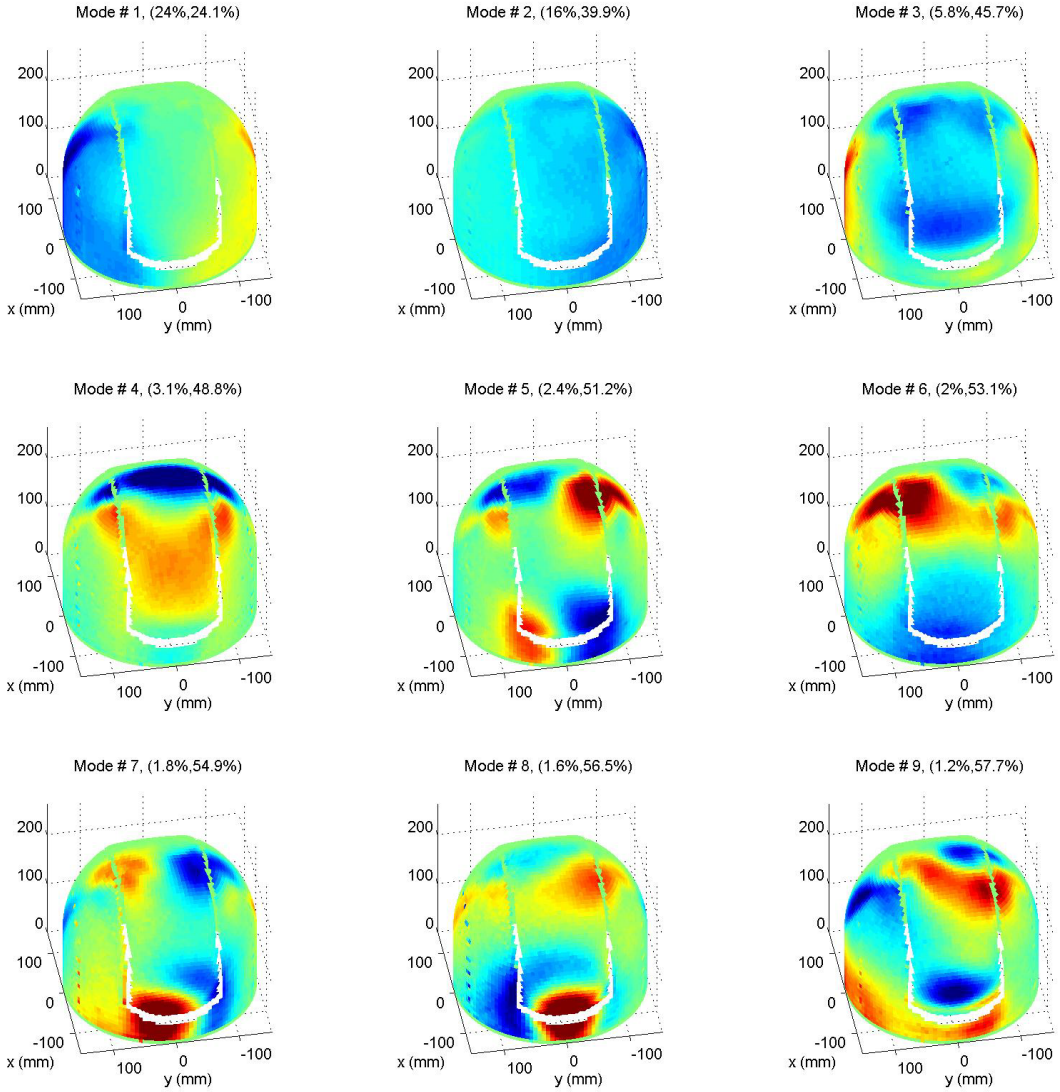

Figure 26. First 9 Joint POD modes for the (0,45)-case. The flow goes along x-axis from positive to negative values. Z-axis is not labeled for clarity.

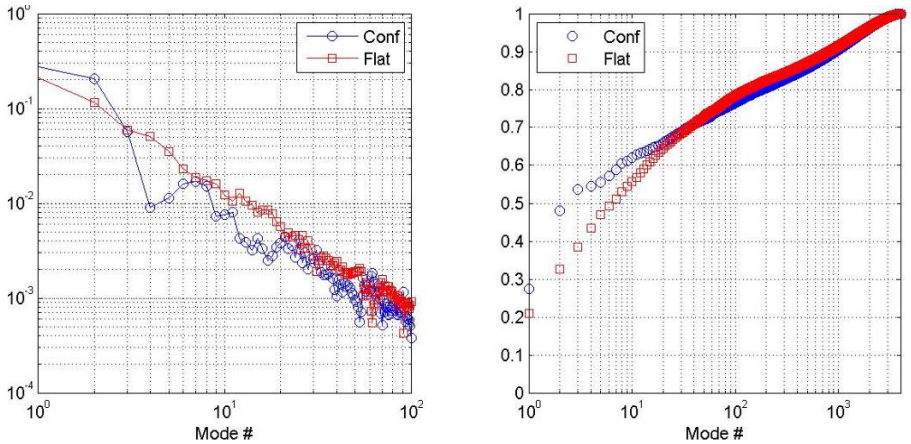

Figure 27. The normalized (left) and normalized cumulative (right) mode energies for the conformal- and flat-window turrets for a joint set of POD modes for (0,45)-case.

Conclusions and Discussion

Fast-response Pressure-Sensitive-Paint technique with multiple high-speed cameras was used to experimentally extract spatially- and temporally-resolved pressure fields for $M = 0.33$ on the surface of the hemisphere-on-cylinder turret with realistic surface features like gaps and "smile" cut-outs for both the conformal- and the flat-window apertures for different window azimuthal/elevation angles. Statistical quantities, like surface maps of the time-averaged pressure standard deviations and instantaneous snapshots of pressure fields were presented, compared and analyzed for different turret geometries. Additionally, a Proper Orthogonal Decomposition was employed to analyze unsteady turbulent pressure structures for different turret geometries and window viewing angles.

The main source of the unsteady pressure variation on the turret was found to be a separation off the downstream portion of the turret. Surface slope discontinuities from "smiles" were also found to significantly affect the instantaneous pressure field, when the "smiles" were located upstream of and close to the separation line, as "smile"-induced separations were found to significantly modify the instantaneous dynamics of the pressure field. For the window azimuthal angle of 0 or 180 degrees, when "smiles" were located at the front and the back of the turret, the overall level of pressure fluctuations on the surface of the turret was found to be minimal. The maximum pressure fluctuations were found for the window azimuthal angle of 90 degrees, when 'smiles" introduced additional strong vortical structures on both sides of the turret downstream of the "smiles", significantly energizing the overall level of unsteady pressure fluctuations.

As the flow was able to travel through small gaps and to form weak jet-like flow though gaps on the downstream potion of the turret, gaps were also found to locally introduce small vortical structures and to modify the instantaneous pressure field near gaps. The slope discontinuity caused by the flat-window aperture also introduced additional localized vortical structures and related pressure fluctuations, when the window was faced either forward or side-ways. Except facing forward, when the flat-window tripped the incoming flow and introduced strong vortical structures on top of the turret, the presence of the flat-window did not significantly changed the overall unsteady pressure field.

POD analysis extracted dominant pressure modes and their temporal coefficients, allowing studying different features of the unsteady pressure field for different window geometries and viewing angles. A joint POD analysis was introduced and it was demonstrated that it provides an alternative approach to compare relative contributions from a joint POD mode to unsteady pressure field for different geometries.

Additional benefit of the POD analysis was a significant noise reduction of the experimentally-extracted pressure fields, providing well-spatially-resolved pressure fields. Also, out of more than 4000 computed POD modes, first 100 POD modes were found to contain all essential information about the pressure field, thus providing very efficient way to compress (by factor of 40) and store data. It shows that POD technique is a very good complementally technique to PSP analysis, as it provides the efficient way to remove noise, store and analyze the spatial-temporal pressure fields.

The Joint POD analysis, although only briefly outlined in the paper for the sake of brevity, was shown to be a powerful systematic way to compare pressure fields for different geometries. In general, the Joint POD can be used to analyze massive spatial-temporal data as a function of some parameter(s), like, geometry, a viewing angle, Reynolds number etc. For instance, it can be useful to quantify the effect of the flow control by identifying modes mostly affected by the flow control.

Knowing spatial distribution of POD modes, a temporal evolution of each mode can be estimated from a sparse unsteady pressure sensor array [24] using LSE approach [25, 26]. Also, the knowledge about spatial distribution of POD modes provides strategies on optimal sensor placement to estimate mode's temporal characteristics [27]. Thus, using a sparse unsteady sensor array, a temporal evolution of dominant pressure POD modes can be estimated and the instantaneous pressure field can be estimated by summing POD modes.

In addition to providing a proper framework to study the time-resolved surface pressure field, POD modes can be useful to study aero-elastic response of the turret, as overall turret mechanical response can be found as a sum of responses to dominant uncorrelated POD modes. In the companion paper [23], POD pressure modes were used to study unsteady forces acting on the turret for different turret geometries and it was found that only first five modes are needed to correctly predict unsteady forces. So, a sparse unsteady pressure array can be properly placed using POD analysis to correctly measure unsteady forces acting on the turret.

All presented measurements were performed at a relatively-low Mach number of 0.33, and small transition effects for the flow around the turret were found to be present at this speed [1,23]. Thus, in order to find a Mach-number-independent POD modes, it is necessary to repeat PSP experiments at a higher Mach number of at least 0.4. Also, the outlined approach to analyze the unsteady pressure fields can be highly-useful at transonic speeds, where additional effects from a local shock on the separated flow from the turret are present [1,28].

Acknowledgments

This work was funded by the Air Force Research Laboratory, Directed Energy Directorate and the High Energy Laser Division of the Joint Technology Office (HEL JTO) and supported by the Air Force Office of Scientific Research through Grant number FA9550-07-1-0574. The U.S. Government is authorized to reproduce and distribute reprints for governmental purposes notwithstanding any copyright notation thereon.

The authors also wish to thank Dr. Jim Crafton of Innovative Scientific Solutions, Inc. for his many useful suggestions about PSP technique.

References

[1] S. Gordeyev and E. Jumper, "Fluid Dynamics and Aero-Optics of Turrets", *Progress in Aerospace Sciences*, 46, (2010), pp. 388-400.

[2] N. De Lucca, S. Gordeyev and E. Jumper, "Comparison of Aero-Optical Measurements from the Flight Test of Full and Hemispherical Turrets on the Airborne Aero-Optics Laboratory", AIAA Paper 2012-2985, 2012.

[3] C. Porter, S. Gordeyev, M. Zenk and E. Jumper, "Flight Measurements of the Aero-Optical Environment around a Flat-Windowed Turret", *AIAA Journal*, Vol. **51**, No. 6, pp. 1394-1403, 2013.

[4] P.E. Morgan, M. D. White and M.R. Visbal," Simulation of Aero-Optics for Flow Over a Flat-Window Hemispherical Turret", AIAA Paper 2011-3264, 2011.

[5] P.E. Morgan and M.R. Visbal," Numerical Simulation of Flow Over a Submerged Hemispherical Flat-Window Turret", AIAA Paper 2012-3042, 2012.

[6] R. Jelic, S. Sherer and R.Greendyke, "Simulation of Various Turret Configurations at Subsonic and Transonic Flight Conditions Using OVERFLOW", AIAA Paper 2012-464, 2012.

[7] P.E. Morgan and M.R. Visbal., "Hybrid Reynolds-Averaged Navier-Stokes/Large-Eddy Simulation Investigating Control of Flow over a Turret", *Journal of Aircraft*, **49**(*6*), pp. 1700-1717, 2012.

[8] B. Vukasinovic, A. Glezer, S Gordeyev and E. Jumper, "Flow Control for Aero-Optics Application", *Experiments in Fluids*, **54**, p. 1492, 2013.

[9] S. Gordeyev, J. Cress, A. Smith and E. Jumper, "Improvement in Optical Environment over Turrets with Flat Window Using Passive Flow Control", AIAA Paper 2010-4492, 2010.

[10] N. De Lucca, S. Gordeyev and E. Jumper, "The Study of Aero-Optical and Mechanical Jitter for Flat Window Turrets", AIAA Paper 2012-0623, 2012.

[11] Liu, T. and Sullivan, J. P., *Pressure and Temperature Sensitive Paints*, Springer, Berlin, 2005.

[12] Gregory, J. W., Asai, K., Kameda, M., Liu, T., and Sullivan, J. P., "A Review of Pressure-Sensitive Paint for High-Speed and Unsteady Aerodynamics," *Proceedings of the Institution of Mechanical Engineers, Part G: Journal of Aerospace Engineering,* Vol. **222**, No. 2, 2008, pp. 249-290.

[13] Gregory, J.W., Sakaue, H., Liu, T., and Sullivan, J. P., "Fast Pressure-Sensitive Paints for Flow and Acoustic Diagnostics," *Annual Review of Fluid Mechanics*, Vol. **46**, 2014.

[14] Fang, S., Long, S. R., Disotell, K. J., Gregory, J. W., Semmelmayer, F. C., and Guyton, R. W., "Comparison of Unsteady Pressure-Sensitive Paint Measurement Techniques," *AIAA Journal*, Vol. 50, No. 1, 2012, pp. 109-122.

[15] Fang, S., Disotell, K. J., Long, S. R., Gregory, J. W., Semmelmayer, F. C., and Guyton, R. W., "Application of Fast-Responding Pressure-Sensitive Paint to a Hemispherical Dome in Unsteady Transonic Flow," *Experiments in Fluids*, Vol. **50**, No. 6, 2011, pp. 1495-1505.

[16] E.J. Jumper, M. Zenk, S. Gordeyev, D. Cavalieri and M.R. Whiteley, "Airborne Aero-Optics Laboratory", *Journal of Optical Engineering*, **52**(7), 071408, 2013.

[17] K. Hird, T. J. Juliano, J, Gregory, N. Delucca, S. Gordeyev, E. Jumper, J. Thordahl and D.J. Wittich," Study of Unsteady Surface Pressure on a Turret via Pressure-Sensitive Paint", AIAA Paper 2013-3135, 2013.

[18] I. Carlbom and J. Paciorek, "Planar Geometric Projections and Viewing Transformations". *ACM Computing Surveys* **10** (4), 465–502, 1978.

[19] R.M. Haralick, "Using Perspective Transformations in Scene Analysis", *Computer Graphics and Image Processing*, Vol. 13, pp. 191-221, 1980.

[20] Tan, T.N., Sullivan, G.D., and Baker, K.D. 1993. On computing the perspective transformation matrix and camera parameters. In Proc. of 4th British Machine Vision Conf., Surrey, England, pp. 125–134.

[21] G. Berkooz, P. Holmes, and J. Lumley, "The Proper Orthogonal Decomposition in the Analysis of Turbulent Flows", *Annual Review of Fluid Mechanics*, Vol. 25, No. 1, pp. 539-575, 1993.

[22] S. Gordeyev, M. Post, T. MacLaughlin, J. Ceniceros and E. Jumper, "Aero-Optical Environment Around a Conformal-Window Turret", *AIAA Journal*, vol. **45**, No. 7, pp. 1514-1524, 2007.
[23] N. Delucca, S. Gordeyev, E. Jumper, K. Hird, T. J. Juliano, J, Gregory, J. Thordahl and D.J. Wittich,"The Estimation of the Unsteady Force Applied to a Turret in Flight", AIAA Paper 2013-3136, 2013.
[24] R.M. Everson, L. Sirovich, "The Karhunen–Loeve transform for incomplete data", *J. Opt. Soc. Am. A* **12** (*8*) 1657–1664, 1995.
[25] Adrian RJ. *On the role of conditional averages in turbulence theory*. In: Zakin J, Patterson G, editors. Proceedings of the Fourth Biennial Symposium on Turbulence in Liquids. Princeton: Science Press, p. 323–32. 1977.
[26] Bonnet JP, Cole DR, Delville J, Glauser MN, Ukeiley LS "Stochastic estimation and proper orthogonal decomposition: complementary techniques for identifying structure", *Exp. Fluids*, **17**, pp.307–314, 1994.
[27] K. Cohen, S. Siegel, D. Wetlesen, J.Camero, and A. Sick "Effective Sensor Placements for the Estimation of Proper Orthogonal Decomposition Mode Coefficients in von Karman Vortex Street", *Journal of Vibration and Control,* **10**(*12*), 1857-1880, 2004.
[28] S. Gordeyev, R. Burns, E. Jumper, S. Gogineni, M. Paul and D.J. Wittich, "Aero-Optical Mitigation of Shocks Around Turrets at Transonic Speeds Using Passive Flow Control", AIAA Paper 2013-0717.